Sussex Research Online

Cl 1205+44: A Fossil Group at z = 0.59

Article (Published Version)

Cl 1205+44: A FOSSIL GROUP AT $z = 0.59$

M. P. Ulmer

Department of Physics and Astronomy, Northwestern University, Evanston, IL 60208-2900; m-ulmer2@northwestern.edu

C. Adami and G. Covone

Laboratoire d'Astrophysique de Marseille, Traverse du Siphon, 13012 Marseille, France;
christophe.adami@oamp.fr, giovanni.covone@oamp.fr

F. Durret

Institut d'Astrophysique de Paris, CNRS, 98 bis Boulevard Arago, 75014 Paris, France; durret@iap.fr

G. B. Lima Neto

Instituto de Astronomia, Geofísica, e Ciências Atmosféricas, Universidade de São Paulo,
Rua do Matão 1226, 05508-090 São Paulo, Brazil; gastao@astro.iag.usp.br

K. Sabirli[1]

Carnegie Mellon University, 5000 Forbes Avenue, Pittsburgh, PA 15213; sabirli@sussex.ac.uk

B. Holden[2]

Department of Physics, University of California, Davis, 1 Shields Avenue, Davis, CA 95616; holden@ucolick.org

R. G. Kron

Fermi National Accelerator Laboratory, MS 127, Box 500, Batavia, IL 60510; rich@oddjob.uchicago.edu

AND

A. K. Romer[1]

Carnegie Mellon University, 5000 Forbes Avenue, Pittsburgh, PA 15213; romer@sussex.ac.uk
Received 2004 August 18; accepted 2005 January 7

ABSTRACT

This is a report of *Chandra*, *XMM-Newton*, *Hubble Space Telescope*, and Astrophysical Research Consortium telescope observations of an extended X-ray source at $z = 0.59$. The apparent member galaxies range from spiral to elliptical, and are all relatively red ($i' - K_s$ about 3). We interpret this object to be a fossil group based on the difference between the brightness of the first and second brightest cluster members in the i' band, and because the rest-frame bolometric X-ray luminosity is about $9.2 \times 10^{43} \, h_{70}^{-2}$ ergs s^{-1}. This makes Cl 1205+44 the highest redshift fossil group yet reported. The system also contains a central double-lobed radio galaxy that appears to be growing via the accretion of smaller galaxies. We discuss the formation and evolution of fossil groups in light of the high redshift of Cl 1205+44.

Subject headings: galaxies: clusters: individual (Cl 1205+44) — X-rays: individual (Cl 1205+44)

Online material: color figures

1. INTRODUCTION

In a *ROSAT* survey of extended sources (Romer et al. 2000; Adami et al. 2000), we found a source with extended X-ray emission with only a single faint optical (*R*-band) counterpart. On deep optical images, the colors of the galaxies in the X-ray area were red enough so that the program HYPERZ derived a photometric redshift greater than 1. This led to *Chandra* and *XMM-Newton* observations of the object, which we designate Cl 1205+44. We find that the system is a fossil group at the highest redshift yet published (0.59 vs. typical values of ≲0.1). The system is particularly interesting because it allows us to explore evolutionary tracks of fossil groups and to consider scenarios for the evolution of galaxies in groups.

Fossil groups have been defined (e.g., Jones et al. 2003) as being similar to groups (poor clusters) in which the luminosity function of the member galaxies has been modified by accretion of galaxies onto the central galaxy while the rest of the system remains unevolved for approximately 4 Gyr. The galaxy accretion onto the D galaxy leads to a magnitude difference between the first and second brightest galaxies (m_{12}) of 2 or higher in the rest-frame *R* or *V* bands within one-half a virial radius, where Jones et al. (2003) use the following to calculate the virial radius: $r_{\mathrm{vir}} = 3.89(T/10 \text{ keV})^{0.5}(1 + z)^{-3}/2 \, h_{50}^{-1}$ Mpc.

Moreover, Cl 1205+44 is interesting because it harbors a double-lobed radio source that is also a D (central dominant) galaxy. Such systems can be directly compared with the model of West (1994). In addition, the radio source simply makes the group more complex, and its formation could be related to cooling flows[3] on one hand and energy injection on the other (e.g., Sun et al. 2003).

A D galaxy that is a radio source is a tracer for finding fossil groups that led J. S. Mulchaey (2003, private communication; see also Mulchaey et al. 2003) independently to identify this object

---

[1] Current address: Astronomy Center, Department of Physics and Astronomy, University of Sussex, Falmer, Brighton BN1 9QH, UK.
[2] Current address: UCO/Lick Observatories, 1156 High Street, Santa Cruz, CA 95065.

[3] Cooling flow literature is too extensive to reference comprehensively; a few references that directly relate radio lobes to X-rays in relatively poor systems with X-ray emission are Carilli et al. (1994), Harris et al. (2000), and McNamara et al. (2000).

as a fossil group and to obtain *Hubble Space Telescope* (*HST*) and redshift observations. The *HST* and redshift data nicely complement the *Chandra*, *XMM-Newton*, i'-, and K_s-band data we have obtained.

Our study of Cl 1205+44 also adds one more data point to the topic of preheating. Recent studies of simulations of preheating can be found, for example, in Borgani et al. (2004). The possibility of preheating of the intracluster medium (ICM) in groups and clusters has taken on added significance, as it relates to the Suyanev-Zel'dovich (SZ) effect, which can influence the interpretation of the high-order power spectrum of the cosmic microwave background (CMB; Lin et al. 2004).

In this paper, we report the results of our multiwavelength analysis and discuss how Cl 1205+44 fits into the larger picture of fossil group formation and evolution.

We use $H_0 = 70$ km s^{-1} Mpc^{-1}, $\Omega_\Lambda = 0.7$, and $\Omega_m = 0.3$ hereafter. At a redshift of 0.5915, which is the most likely redshift of Cl 1205+44, the angular scale for this cosmology is 6.64 kpc arcsec^{-1}.

2. OBSERVATIONS AND ANALYSIS

2.1. *Optical-IR Observations*

We made observations in the i' and K_s bands at the Astrophysical Research Consortium telescope.[4] For the i' band, we used the SPIcam camera for a net total exposure time of 7200 s at a mean air mass of 1.15, and for the K_s band we used the GRIMII camera for a net total exposure time of 7200 s. We took separate 10 minute exposures to acquire the i'-band data and took 10–30 s exposures to accumulate the K_s data. The i'-band data were reduced using the ESO-MIDAS package, and the K_s data were reduced using DIMSUM, an NOAO/IRAF tool. The zero points were computed using standard stars observed at the same time as the scientific data and at similar air masses.

The *HST* data were retrieved from the archive (proposal ID: 8131, PI: Mulchaey). They consist of six 1200 s dithered *R*-band WFPC2 (F702W filter) exposures. We reduced the data using the DRIZZLE IRAF package (Fruchter & Hook 2002). We generated catalogs of detected objects using SExtractor (ver. 2.3; Bertin & Arnouts 1996) using a detection threshold of 1.5 σ and an analysis threshold of 2 σ.

We used the fixed aperture 3″ mag from SExtractor for the *HST* magnitudes, and we used the SExtractor automagnitude feature to derive the magnitudes for the ARC data. Figure 1 gives the magnitude histograms in the three magnitude bands available to us: in the ARC SPIcam field of view for i', in the ARC GRIMII field of view for K_s, and in the *HST* WFPC2 field of view for F702W. These histograms allow us to estimate an upper limit to the completeness value of the magnitude in each band: $i' \sim 22.25$, F702W ~ 26.25, and $K_s \sim 19.75$. The respective solid angle coverage of the instruments is as follows: WFPC2 image, 2.2×2.2 arcmin^2; i' image, 6×4.3 arcmin^2; and K_s image, 2×2 arcmin^2.

In order to assess the quality of our data, we plotted the magnitudes in the different bands against each other, as shown in Figure 2. We estimate from the results a relative 1 σ uncertainty between magnitudes (limiting ourselves to the brightest completeness limit) of 0.26 mag between F702W and i' and of 0.36 mag between i' and K_s. This gives an upper limit to the magnitude uncertainty, since some of the scatter is due to the intrinsic color variations of the objects.

As an external test, we compared our K_s magnitudes with the estimates for the two objects in the K_s field bright enough to be
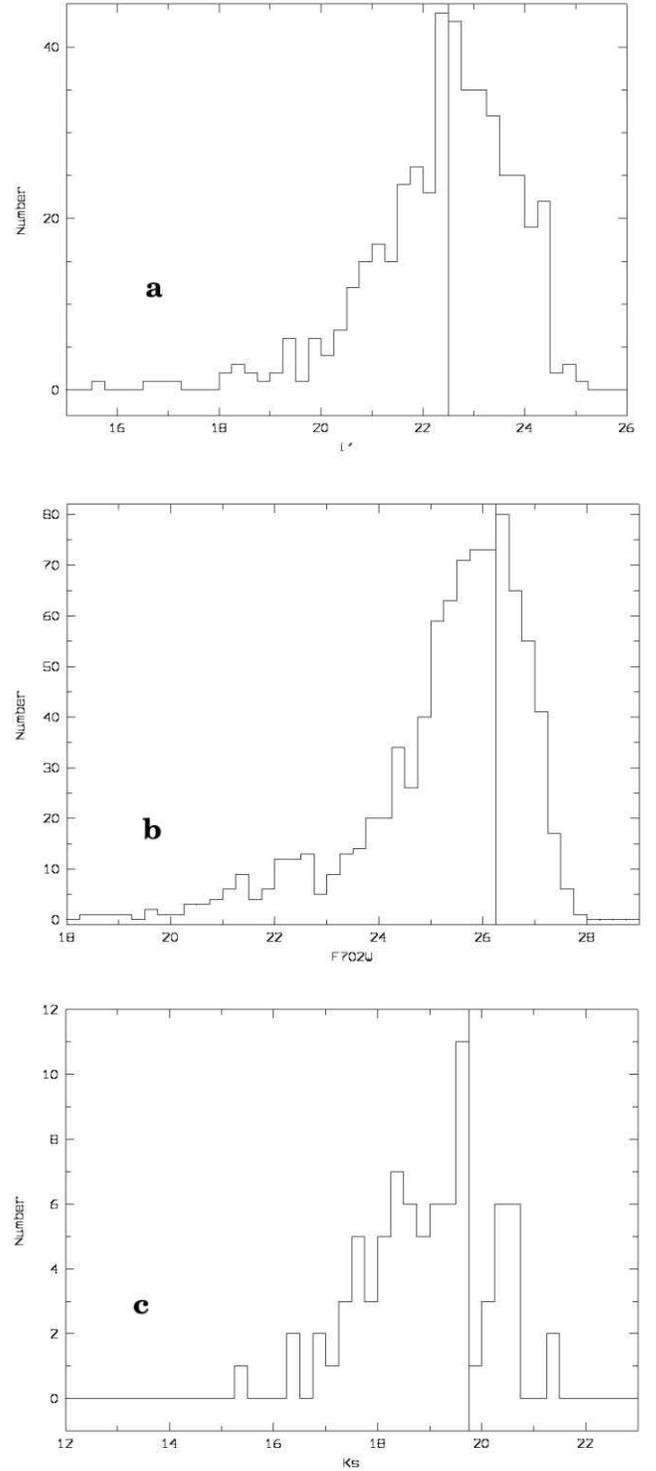
Fig. 1.—Histograms of the total magnitudes in the ARC SPIcam field of view for i', in the *HST* WFPC2 field of view for F702W, and in the ARC GRIMII field of view for K_s. The vertical lines give the upper limits for the completeness: $i' \sim 22.25$, F702W ~ 26.25, and $K_s \sim 19.75$.

detected by 2MASS[5] (including the D galaxy). We have reasonable agreement (for the two objects, $K_s - K_{2\mathrm{MASS}} = -0.38$ and $+0.26$) given that these objects are below the 2MASS completeness limit.

For use in our discussion below, we calculated the total *R*-band luminosity. To derive this number, we used the total

FIG. 3.—*Chandra* contours from the 0.5–8 keV image superposed on the F702W *HST* image of Cl 1205+44. We used a smoothing window for the contours of 4″.5, which is a finer scale than we used in Figs. 10 and 11. North is up, and east is to the left.

F702W flux enclosed[6] by the X-ray contours in Figure 3. We estimate that approximately 90% of our derived value of L_R comes from the galaxies enclosed by rectangles in Figure 4. Therefore, the L_R value is probably accurate to within 20%. The 20% uncertainly is also consistent with subtracting the flux of galaxy 6 in Figure 3 (see also Table 1), which, based on its colors, is the most likely in our list not to be a cluster member. The uncertainty in L_R does not affect any conclusion we draw in § 4. The F702W total luminosity is $6.0 \times 10^{11} \ L_\odot$. Converting to

[6] We excluded the star, which is the brightest object toward the top of the figure but inside the contours; it is south-southwest of the D galaxy.
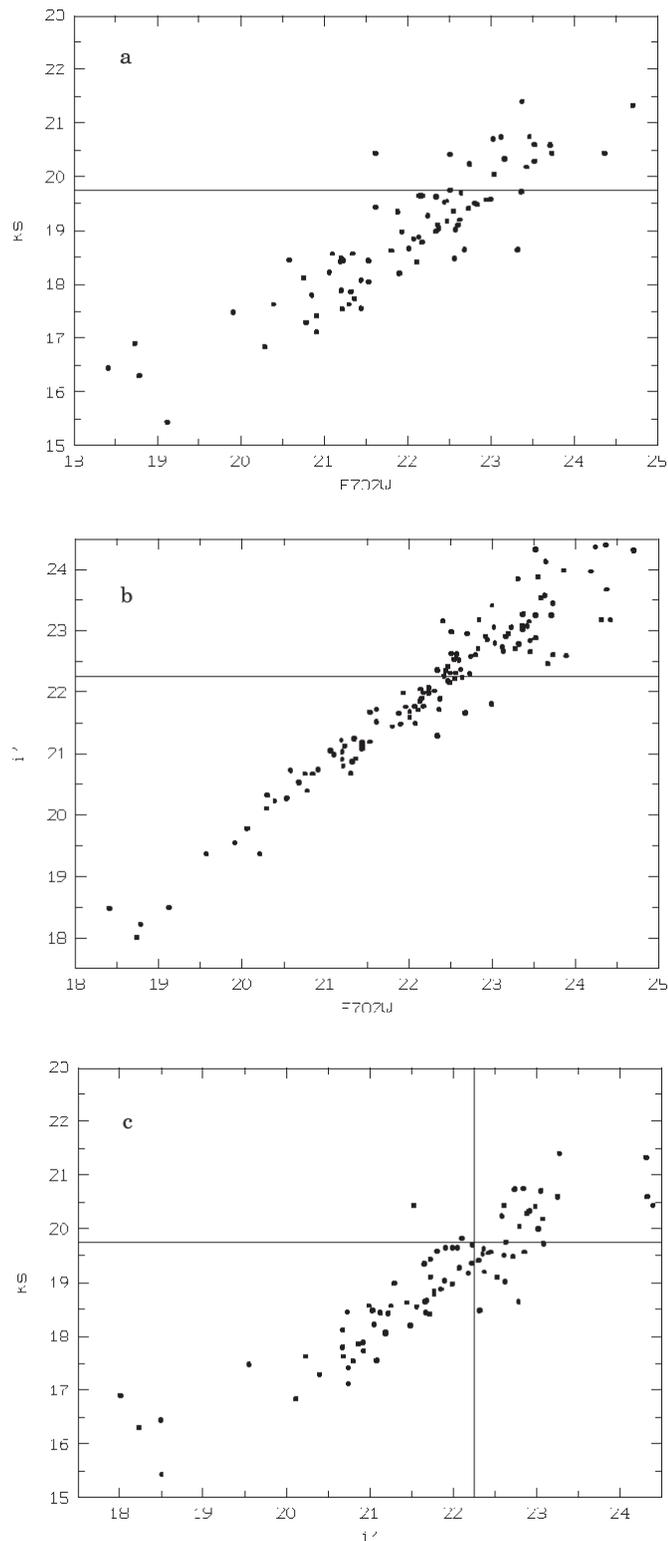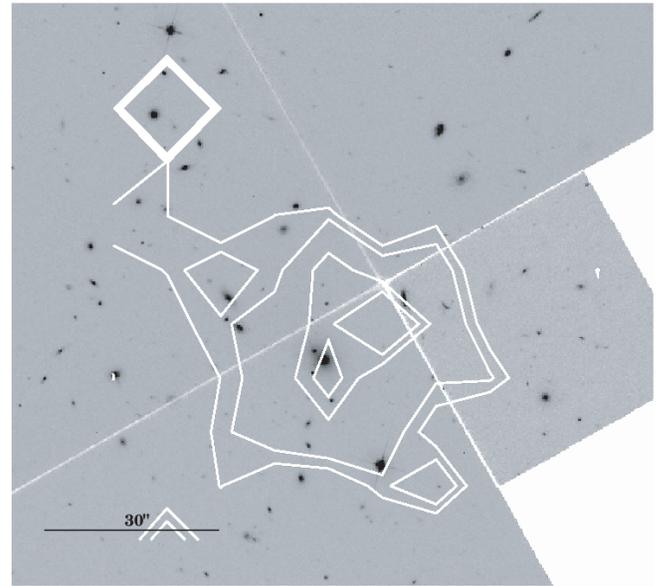

FIG. 2.—Relation between our three magnitudes plotted against each other two at a time. The horizontal lines and vertical line show the completeness levels for the i' and K_s data taken from in Fig. 1.
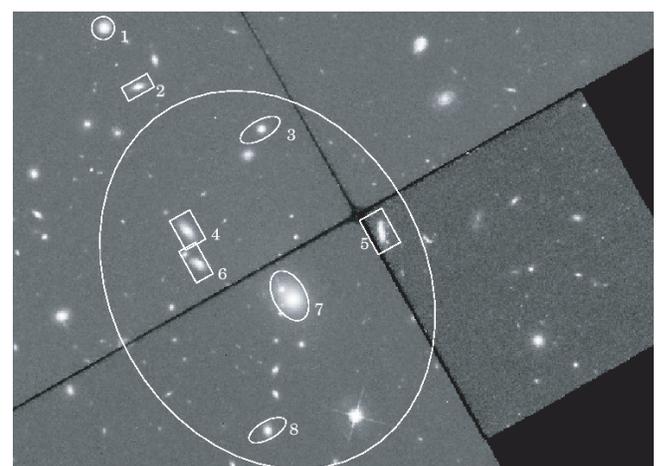
FIG. 4.—Expanded image of the *HST* $\sim 0'.97 \times 0'.72$ field. North is up, and east is to the left. The northernmost circled galaxy is likely to be a line-of-sight AGN. The galaxies marked with rectangles are late types, and those with ellipses are early types. The large ellipse represents the approximate extent of the X-ray emission; see Fig. 3 for a more accurate superposition of the X-ray flux onto the *HST* image. Starting from the north, AGN, the respective i' ID numbers to correlate with Table 1 i' magnitudes and $(K_s - i')$ values are: (1) 18.23 (1.93); (2) 20.80 (3.26); (3) 21.19 (3.14); (4) 20.43 (3.14); (5) 20.65 (3.02); (6) 20.99 (2.42); (7) 18.50 (3.06); and (8) 20.85 (2.99).

TABLE 1
PROBABLE GROUP MEMBERS

ID (Class)[a]	R.A. (deg)	Decl. (deg)	F702W	i'	K_s
1 (AGN)[b]	181.474	44.4960	19.27	18.23	16.30
2 (S)	181.472	44.4938	21.04	20.80	17.54
3 (E)	181.466	44.4923	21.38	21.19	18.05
4 (S)	181.470	44.4885	20.73	20.43	17.29
5 (S)	181.460	44.4885	21.84	20.65	17.63
6 (S)[c]	181.469	44.4873	21.01	20.99	18.57
7 (D)	181.464	44.4860	19.27	18.50	15.44
8 (E)	181.465	44.4812	21.22	20.85	17.85

[a] Includes identification number (ID) and classification as either AGN, spiral galaxy (S), or elliptical galaxy (E).
[b] Assumed not to be a group member, but included for comparison and completeness. This object is a point X-ray source, as seen in Fig. 11.
[c] Possibly not a group member; see text.

the R_J band used by Jones et al. (2003), we obtain $L_R = 5.5 \times 10^{11} \ L_\odot$. The K-correction to $z = 0$ gives a (rest frame) value of $L_R = 7.8 \times 10^{11} \ L_\odot$. Finally, to compare with Jones et al., we use $H_0 = 50$ and $q_0 = 0.5$, which leads to $L_R = 8.9 \times 10^{11} \ L_\odot$.

2.2. Redshift

Since the X-ray data were not of sufficient signal-to-noise ratio to constrain the cluster redshift (see below), we needed optical spectra of the galaxies belonging to the system. By chance, this system was observed by J. S. Mulchaey (2003, private communication) in his ongoing fossil group survey, and he kindly provided us with the value of the redshift of the brightest galaxy of the putative fossil group, $z = 0.5915$. These data, plus the positional coincidence of the brightest group galaxy (hereafter D galaxy) with the centroid (see § 2.3.4) of the X-ray emission, firmly identifies the extended X-ray emission with the brightest galaxy and the associated galaxies in Table 1.

2.3. X-Ray Observations

We were granted time to observe Cl 1205+44 with *XMM-Newton* (2003 June; 52,200 s) and *Chandra* (2003 October; 31,800 s).

2.3.1. Chandra Data

The *Chandra* observation was made in very faint mode, with a time resolution of 3.24 s and a CCD temperature of -120°C. The data were reduced using CIAO, version 3.0.1,[7] following the Standard Data Processing, producing new Level 1 and 2 event files.

We further filtered the Level 2 event file, keeping only *ASCA* grades 0, 2, 3, 4, and 6, and restricted our data reduction and analysis to the back-illuminated chip, ACIS-S3. We checked that no afterglow was present and applied the Good Time Intervals (GTI) supplied by the pipeline. Then we checked for flares using the light curve in the 10–12 keV band; no flare was detected, and the total exposure time was 29,711 s.

We used the CTI-corrected ACIS background event files ("blank-sky"), produced by the ACIS calibration team,[8] available from the calibration database (CALDB). The background events were filtered, keeping the same grades as the source events, and were then reprojected to match the sky coordinates of the Cl 1205+44 ACIS observation.

[7] See http://asc.harvard.edu/ciao.
[8] See http://cxc.harvard.edu/cal/Acis/WWWacis_cal.html.

TABLE 2
PHOTON COUNT PER DETECTOR

Count	MOS1	MOS2	pn	ACIS
Total[a]	180	153	458	465
Cluster	147	117	381	295

[a] Total: cluster + background. These counts were used for the fitting of the spectra from the cleaned event files and within the energy ranges described in § 2.3.3.

2.3.2. XMM-Newton Data

Cl 1205+44 was observed in standard Full Frame mode, using the "thin" filter with the two EPIC MOS1 and MOS2 and the pn detectors. The basic data processing (the "pipeline" removal of bad pixels, electronic noise, and correction for charge transfer losses) was done with SAS, version 5.3, thus creating calibrated event files for each detector.

For the MOS1 and MOS2 cameras, following the standard procedure, we discarded the events with FLAG $\neq 0$ and PATTERN > 12; for the pn, we restricted the analysis to the events with PATTERN ≤ 4 and FLAG $= 0$.

The light curves in the 10–12 keV band that we produced showed that there were severe flaring events during the observation. Filtering out the periods with flares substantially reduced the exposure times: 21,223, 20,861, and 16,478 s for MOS1, MOS2, and pn, respectively (from an initial 52.2 ks).

With the cleaned event files, we created the redistribution matrix file (RMF) and ancillary response file (ARF) with the SAS tasks *rmfgen* and *arfgen* for each camera and for each region that we analyzed.

The background was taken into account by extracting spectra from the blank sky templates described by Lumb et al. (2002) and then reprojected to the same coordinates and roll angle of the Cl 1205+44 *XMM-Newton* observation. The same filtering procedure was applied to the background event files. We give a breakdown of the number of counts used per detector in the fitting in Table 2.

2.3.3. X-Ray Spectral Fits

Spectra were analyzed with XSPEC, version 11.3. We simultaneously fitted all four spectra from the *XMM-Newton* MOS1, MOS2, pn, and *Chandra* ACIS-S3 cameras. The spectra were rebinned so that we could use the standard χ^2 minimization when fitting the spectra. We then applied the MEKAL plasma spectral model (Kaastra & Mewe 1993; Liedahl et al. 1995).

The photoelectric absorption (mainly because of neutral hydrogen in our Galaxy) was computed using the cross sections given by Balucinska-Church & McCammon (1992), available in XSPEC. Given the low count rate, the hydrogen column density N_H could not be well constrained by the spectral fit; therefore, we fixed it to the galactic value at the cluster position. The interpolation of the H I map of Dickey & Lockman (1990), using the task *nh* from FTOOLS, yields $N_H = 1.27 \times 10^{20}$ cm^{-2}. The results are shown in Figure 5. The metallicity is poorly constrained; as shown in Table 3, at a 1 σ confidence level we found $Z < 0.6 \ Z_\odot$ and, at a 90% confidence level, $Z < 1.1 \ Z_\odot$. For completeness in Figure 6 we show how N_H and metallicity correlate with kT in the spectral fits.

We restricted the spectral analysis within the energy range where the cluster emission was above the background and the detectors were well calibrated. For the MOS1 and 2 cameras, this interval was 0.3–8.0 keV, for the pn (0.5–8.0 keV) and for ACIS-S3 (0.4–7.0 keV). The spectra were extracted inside a
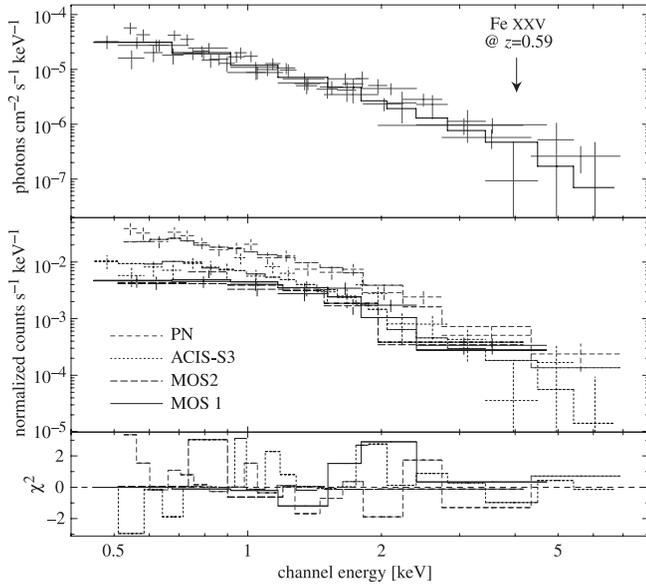
Fig. 5.—*Top*: Flux in photons cm^{-2} s^{-1} keV^{-1}, with data points from all cameras. For simplicity (in the print version), there is only one line drawn of the best-fit spectrum. Except for the lowest energy bin, which is dominated by the MOS data, the fit is dominated by the pn data. The redshifted Fe XXV line for $z = 0.59$ is indicated. *Middle*: Fluxes in counts s^{-1} keV^{-1} for all cameras: *solid line*, MOS1; *long-dashed line*, MOS2; *dotted line*, pn; *short-dashed line*, ACIS-S3. The differences among best-fit spectra come from the different detector responses. *Bottom*: Residues given as the χ^2 contribution of each energy bin. [*See the electronic edition of the Journal for a color version of this figure.*]

Fig. 6.—Probability contours of metallicity and N_H vs. kT fits to the X-ray data; see text.

circle of 1$'$.4 radius, centered on the cluster. The strong northeast X-ray point source (probably an active galactic nucleus [AGN]) is outside this radius.

2.3.4. *X-Ray Luminosity*

For the reasons stated above (§ 2.2), we assume that the cluster redshift is $z = 0.5915$ and fix this value hereafter. Table 3 summarizes the best spectral fits, either fixing the metallicity or the hydrogen column density or both. Clearly, the metallicity is not well constrained, and we only have upper limits for N_H. Fixing the metallicity to the typical value found in clusters (e.g., Fukazawa et al. 2000; 0.3 $Z_\odot$) and N_H to the galactic value, the mean temperature is $kT = 3.0^{+0.3}_{-0.3}$ keV. This system therefore has an X-ray temperature typical of a poor cluster (such as A194, which has a temperature of 2.6 ± 0.15 keV [Nikogossyan et al. 1999], and the poor cluster RX J0848+ 4456, which has a temperature of 3.2 ± 0.3 keV [Holden et al. 2001]) and warmer than that of a typical fossil group (e.g., Jones et al. 2003).

With redshift $z = 0.5915$, the corresponding unabsorbed luminosity and flux in the 2.0–10.0 keV band are $(3.3 \pm 0.3)\ h_{70}^{-2} \times 10^{43}$ ergs s^{-1} and $(1.5 \pm 0.2) \times 10^{-14}$ ergs s^{-1} cm^{-2}. The bolo-

metric luminosity is $(9.2 \pm 0.4)\ h_{70}^{-2} \times 10^{43}$ ergs s^{-1}. The cluster properties are summarized in Table 4. We define the position of the cluster in to be that of the D galaxy, as there is a peak in the contours (see Fig. 3) at this location.

For its measured bolometric luminosity, Cl 1205+44 is hotter than the best fit to the local L_X-T_X relation based on two fossil groups (Jones et al. 2003; see our Fig. 7) but agrees with the local relation of Novicki et al. (2002), and the value falls within $1\ \sigma$ of the L_X-T_X no-evolution relation derived for the $\langle z \rangle = 0.34$ sample of Novicki et al. (2002). For the purpose of later discussion, we have plotted the values of kT versus L_X for Cl 1205+44 on figures taken from Jones et al. and Novicki et al. in our Figures 7 and 8.

2.3.5. *X-Ray Surface Brightness Fits*

We carried out a standard β surface brightness fit to both the *XMM-Newton* data and the *XMM-Newton* plus *Chandra* data combined. We used the 0.5–8 keV bands in both cases. Then with $I_x(b) \propto [1 + (b/r_c)^2]^{-3\beta + 1/2}$ (e.g., Sarazin 1986), where I_b is the surface brightness as function of projected radius b and r_c is the core radius. For the more robust *XMM-Newton* data alone case we found, using a maximum likelihood method, $\beta = 0.45 \pm 0.02$ and $r_c = 21'' \pm 3''$, 1 σ errors. The fit appears better to the eye (see Figs. 9a and 9b) for the *XMM-Newton* plus *Chandra* case, but we found the results so sensitive to the normalization between the two data sets and the binning of the data, that we only quote this fit as a 2 σ lower bound to the core radius = 15$''$; the β was again 0.45 for this minimum χ^2 fit.

2.4. *Radio Source*

The central peak within the second highest contour level in Figure 3 is located on the D galaxy. The D galaxy is also a double-lobed FIRST (White et al. 1998) radio source F1205+ 44 (see Fig. 10) of total flux = 56.4 ± 1.7 mJy at 20 cm (Condon et al. 2002). These facts are relevant to the model proposed by

TABLE 3
THERMAL PLASMA BEST-FIT PARAMETERS

kT (keV)	Z ($Z_\odot$)	N_H (10^{20} cm^{-2})	χ^2/dof
$3.0^{+0.5}_{-0.4}$	$0.30^{+0.30}_{-0.24}$	<3.77	48.02/46
$3.0^{+0.3}_{-0.3}$	$0.30^{+0.30}_{-0.23}$	1.27[a]	48.03/47
$3.0^{+0.5}_{-0.4}$	0.30[a]	<3.53	48.02/47
$3.0^{+0.3}_{-0.3}$	0.30[a]	1.27[a]	48.03/48

NOTES.—Temperature (kT), metallicity (Z), and hydrogen column density (N_H); dof are the degrees of freedom for a given spectral fit.
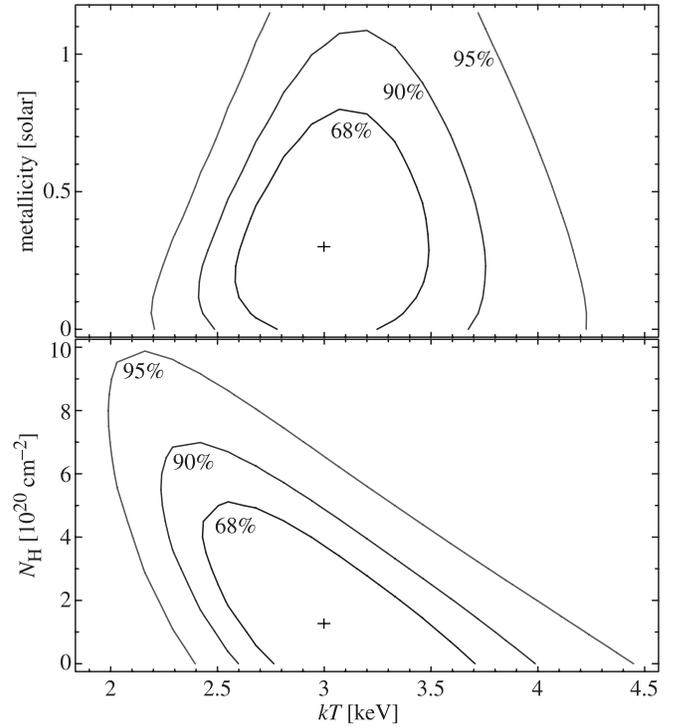[a] Fixed value.

TABLE 4

Main Characteristics of Cl 1205+44

z	α[a] (deg)	δ[a] (deg)	X-Ray Diameter	L_X ($h_{70}^{-2} \times 10^{43}$ ergs s^{-1})	T_X (keV)	L_{opt} (F702W) ($10^{11} L_\odot$)
0.5915........................	181.4641	44.4860	40″	9.2 ± 0.7	3.0 ± 0.3	1.5

[a] J2000.0.

West (1994). He proposed an anisotropic merger model for the origin of the formation of D galaxies, and the model predicts that the D galaxy will be associated with a powerful radio source, which is the case here. Furthermore, the model predicts that the radio lobes will be aligned with the major axis of the X-ray emission in the cluster. Therefore, we attempted to determine the major axis of the X-ray emission, which is rather ill defined. In order to make a determination of the major axis, we heavily smoothed[9] the data to produce Figure 11 (see also Fig. 10). Then, the major axis of the X-ray emission of Cl 1205+44 can be defined by the line joining points A and B in Figure 11. In this case the radio lobe axis is aligned within 10° of the X-ray axis, which is also consistent with the model of West; however, the optical axis of the D galaxy is offset by about 30° with respect to the radio lobe axis, and the West model also predicts alignment with the galaxy distribution. *If* there *is* a galaxy distribution that defines a direction, it is the almost north-south line of galaxies running from galaxies 7 to

___

[9] Note that the heavy smoothing causes the center of second highest contour level in the X-ray emission to be different from that in Fig. 3, but the exact position of the X-ray peak is not important. This is because it is extremely unlikely that the D galaxy would fall so close to the center of this X-ray emission and *not* be associated with the X-ray emission. The highest contour level has two peaks, one of which falls on the D galaxy; see the print version of Fig. 10 or the online image of Fig. 11.

8 in Figure 4. Overall, then, the data are not consistent with the model of West.

3. DISCUSSION

3.1. *Nature of the System*

The most compelling reason for calling Cl 1205+44 a fossil group is because the value of m_{12} within one-half the projected virial radius[10] is very close to that of the Jones et al. (2003) criterion of being >2 for $z \sim 0$ (for the R- or V-band rest frame), i.e., m_{12} $i' = 1.93$. In addition, that the value of m_{12} is slightly smaller can be attributed to Cl 1205+44 being *younger* (by up to

___

[10] For consistency with Jones et al. $r_{vir} = 70''$ we used their cosmology, $H_0 = 50$, $q_0 = 0.5$; then the scale is 7.57 kpc arcsec^{-1}, and from their formula for the virial radius, reproduced in the introduction, $r_{vir}/2 = 0.53 \, h_{50}^{-1}$ Mpc, which corresponds to 70″.
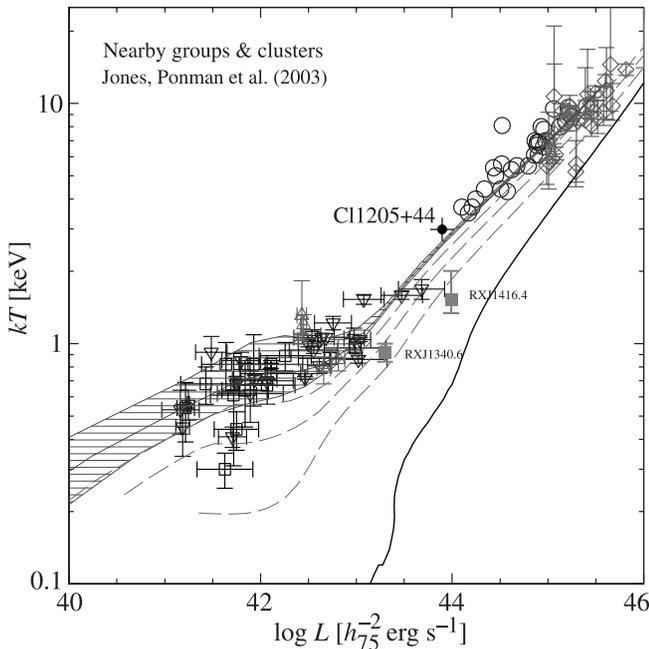

Fig. 7.—Fig. 3 of Jones et al. (2003) with Cl 1205+44 indicated. The solid lines and hatched area are predictions from Babul et al. (2002) based on a preheating entropy of $kTn_e^{-2/3} \simeq 427$ keV cm^2, and the dashed curves are the predictions for 300, 200, and 100 keV cm^2. The lowest curve best fits the two *ROSAT* data points for fossil groups annotated with RXJ names. See Jones et al. for details.
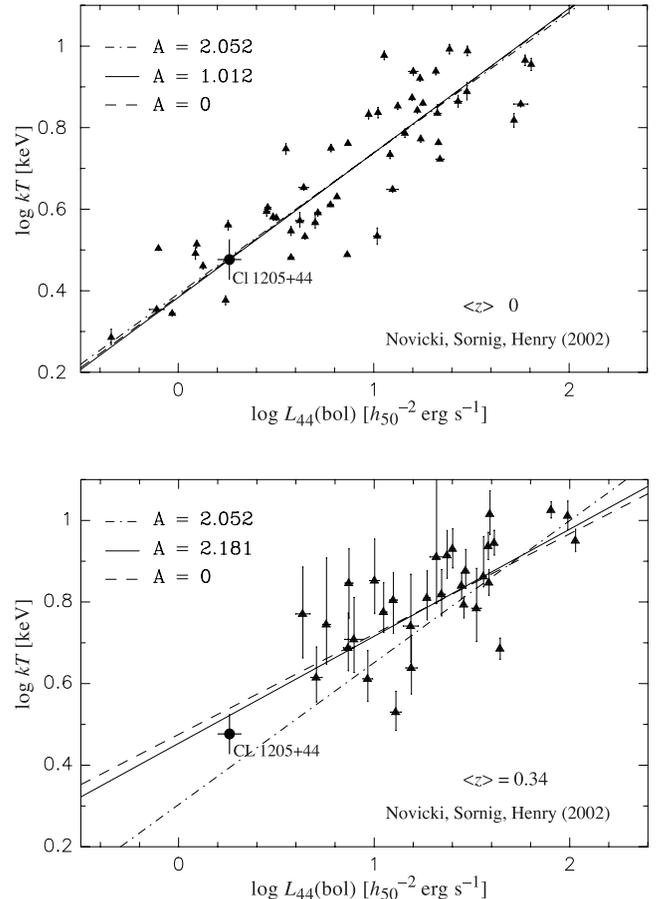

Fig. 8.—Shows the L_X-T_X relation of Novicki et al. (2002) for $z \sim 0$ (*top*: low-redshift data set and solutions, $\Omega_M = 0.3$, $\Omega_\Lambda = 0.7$) and $z \sim 0.3$ (*bottom*: high-redshift data set and solutions, $\Omega_M = 0.3$, $\Omega_\Lambda = 0.7$). Cl 1205+44 is plotted in both figures. The dashed lines in both figures corresponds to the no-evolution model.
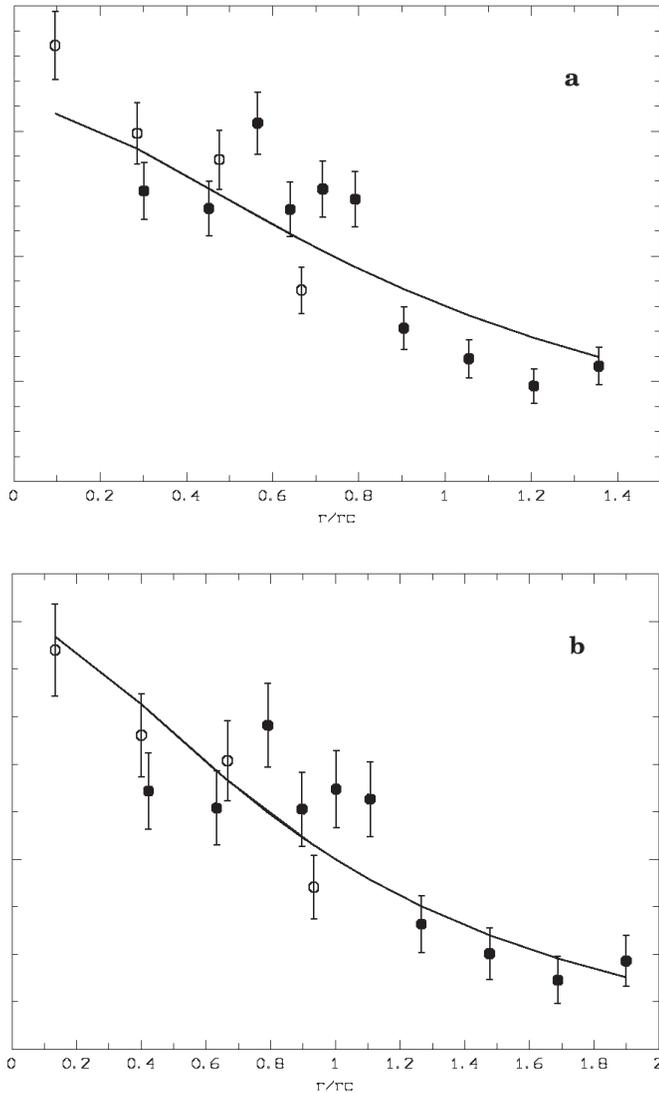
FIG. 9.—(*a*) Radial surface brightness profile fit based on the *XMM-Newton* data (*filled circles*) and the normalized *Chandra* data (*open circles*) in arbitrary units on the *y*-axis. The *x*-axis is in units of r_c. The best fit (*solid curve*) and redshift correspond to ~140 kpc. (*b*) Fit for the combined data set; here the core radius corresponds to a ~100 kpc. See text.
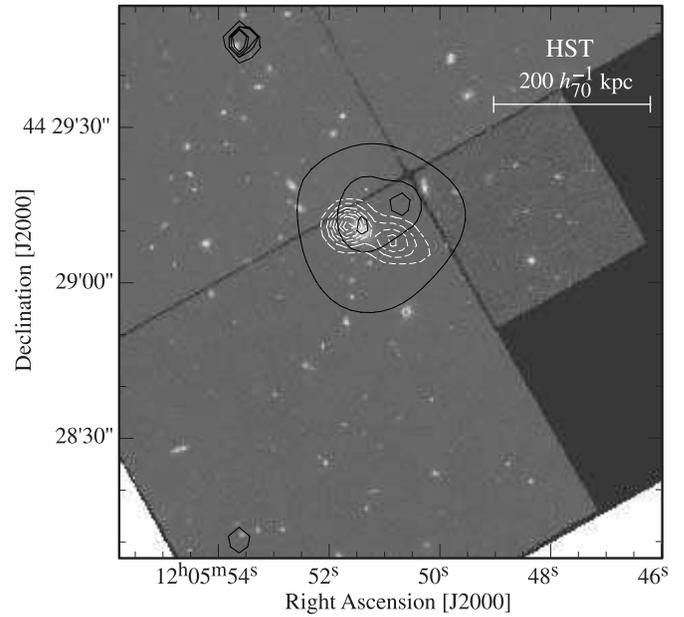

FIG. 10.—*Chandra* solid contours from the 0.5–8 keV image (see also Fig. 11) superposed on the F702W *HST* image of Cl 1205+44 along with the dashed contours for the FIRST double-lobed radio source. North is up, and east is to the left. [*See the electronic edition of the Journal for a color version of this figure.*]
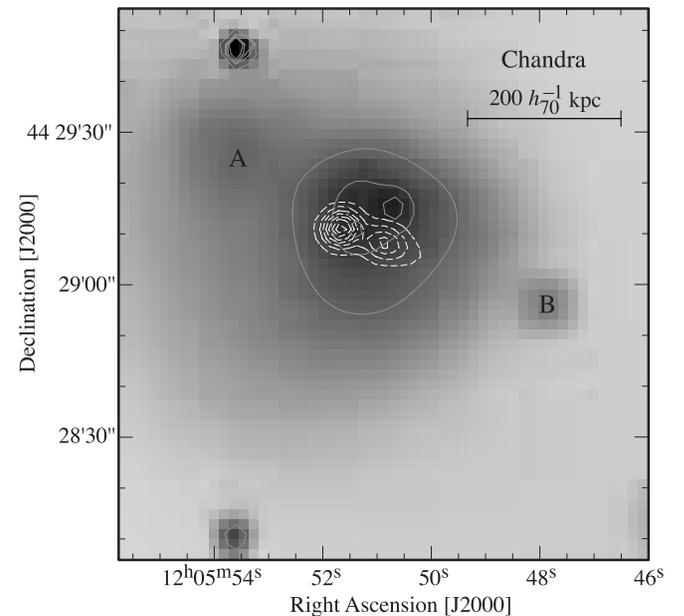

FIG. 11.—*Chandra* solid contours superposed to a smoothed *Chandra* 0.5–8 keV image of Cl 1205+44 along with the dashed contours of the FIRST double-lobed radio source. The *Chandra* data are logarithmically spaced, and the radio contours are linearly spaced. The *Chandra* image (rebinned by a factor of 4, i.e., 1 pixel = 2″) is adaptively smoothed using the task *csmooth* from CIAO, ver. 3, corrected by the exposure map. The X-ray contours that appear on the cluster are linearly spaced at 4, 8, and 12 σ above the background (i.e., the more or less circular contour is 4 σ above the background; the two peaks are 12 σ above the background). Then the contour levels go geometrically (those over the AGN go geometrically). The color scale map, however, is logarithmic. The VLA FIRST contours are linearly spaced, beginning at 0.0035 Jy beam^{-1} in steps of 0.0035 Jy beam^{-1}. North is up, and east is to the left. The point sources at the top and bottom of the image to the east of center are line-of-sight objects that are probably AGNs not associated with Cl 1205+44. [*See the electronic edition of the Journal for a color version of this figure.*]

~4 Gyr) than $z = 0$ fossil groups; in the Jones et al. scenario, the central galaxy grows in brightness with time as it accretes more galaxies. In older systems the central galaxy will have had more time to accrete galaxies and hence be brighter compared to the remaining ones.

The X-ray–emitting AGN we have listed in Table 1 is brighter than the D galaxy in the *i*′ band, so if it were a cluster member, then Cl 1205+44 would certainly not be fossil group. However, we have (without redshifts) two arguments against this AGN being a group member: (1) its color is significantly bluer than the other (probable) cluster members in Table 1, and (2) the AGN becomes the dominant galaxy and is then $\gtrsim 2$ (X-ray) core radii away from centroid of the extended X-ray emission.

To be a fossil group, the lower limit Jones et al. (2003) place on $L_{\mathrm{X\,bol}}$ is 1×10^{42} h_{50}^{-2} ergs s^{-1}, which Cl 1205+44 easily meets. Although Jones et al. do not set an upper limit to the kT or X-ray luminosity, the $L_{\mathrm{X\,bol}}$ (corrected to $H_0 = 75$ for their Fig. 3 and our Fig. 7) point falls in the region where the Jones et al. fossil group sample lies. Cl 1205+44 is also distinguished from "normal clusters" in that the $L_{\mathrm{X\,bol}}$ value is about a factor
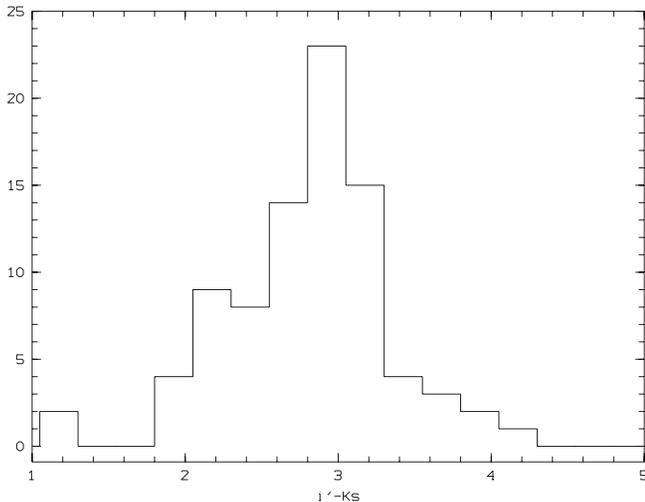
FIG. 12.—Histogram of the $i' - K_s$ colors. Luminous galaxies at $z \sim 0.59$ have similar colors according to a correlation between SDSS and 2MASS photometry.

of 2 lower at $kT \sim 3$ keV than the cluster sample complied by Lumb et al. (2004) for clusters at $z \sim 0.4$–0.6. In contrast, the $L_{\mathrm{X\,bol}}$-L_R point lies approximately halfway between the Jones et al. lines for "normal" X-ray–bright groups and fossil groups. In addition, the X-ray luminosity and kT values are similar to the values Holden et al. (2001) assigned to an extended X-ray–emitting region that they simply classified as a "cluster." In the end, however, the m_{12} value of nearly 2 (within one-half the projected r_{vir}) and $L_{\mathrm{X\,bol}} > 10^{42}$ ergs s^{-1} meet the primary Jones et al. criteria, which leads us to conclude that Cl 1205+44 is a fossil group, and we assume that it is a fossil group in what follows.

3.2. *Fossil Group Members*

We must make an assumption about galaxy membership as redshifts for the specific galaxies are not available to us, and except for the D galaxy, none of those marked in Figure 4 were measured by J. S. Mulchaey (2003, private communication). The conclusion that these galaxies are all group members is based on the following: their i' magnitudes are all similar except for the D galaxy; their colors are all similar except for galaxy 6; their apparent sizes are all similar; and their average color (see also § 3.6) corresponds to the peak in the histogram of the $i' - K_s$ distribution shown in Figure 12. We assume, therefore, that except for 6, all these galaxies are cluster members. Based on their disklike morphology, we classified three out of the six group members as late-type (spiral) galaxies, and the other three (including the D galaxy) as early-type (elliptical) galaxies. We will refer to the galaxy population and colors in our discussion of the scenarios of this fossil group formation in §§ 3.6 and 3.8.

3.3. *Possible Cooling Evolution*

Perhaps the reason that Cl 1205+44 is hotter than the two $z = 0$ fossil groups with measured temperatures discussed by Jones et al. (2003) is because of cooling between $z \sim 0.6$ and 0. We now consider this possibility. We used the cooling time equation from Sarazin (1986) for our calculations (see § 3.5 for details). To derive a lower bound, we used our $\beta = 0.45$, $r_c = 15''$ model fit, and we derived an average cooling time of 6.5 Gyr within $1r_c$ and ~ 11 Gyr within $2r_c$. The time between $z = 0.59$ and 0.2 (the highest redshift in on which Jones et al. base their discussion of fossil groups formation and evolution)

is only 3 Gyr. Even the longer time of 4 Gyr (the average age of fossil group in the Jones et al. scenario) is less than the 6.5 Gyr we derived for the average cooling time within the core. We derive a 2 σ lower bound of ~ 4 Gyr at the very core, which could lead to cooling in the center of the cluster. It is unlikely, therefore, that the ICM of high-redshift fossil groups is hotter than low-redshift ones because of cooling between $z \sim 0.6$ and 0.0. We defer a discussion of the energy input to the ICM until § 3.8.1.

The issue of cooling, gas infall (or the suppression of gas infall), resulting heating due to gas infall, etc., is a complicated one and has been discussed extensively in the literature; see, for example, some recent works (Clarke et al. 2004; Kaastra et al. 2004; Peterson et al. 2004 and references therein). The purpose of the above discussion was not to argue for or against cooling per se, but rather to determine whether is possible for the gas to have cooled enough between $z \sim 0.6$ and 0.1 to explain the temperature differential between Cl 1205+44 and nearby fossil groups. We have shown that if we assume the simplest circumstances, of a collisionless gas without a tangled magnetic field, that the gas could just barely cool over this $z \sim 0.6$–0.1 time frame. Then, since heat input is likely in any event, we conclude that the nearby fossil groups do *not* have lower temperatures than Cl 1205+44 because of cooling. It may just be that hot fossil groups such as Cl 1205+44 are rare per unit volume, but these are the ones that are easiest to detect at high z.

3.4. *The Radio and X-Ray Source Relation*

The issue is whether or not there is evidence for the radio source interacting with the ICM and/or producing X-rays via the inverse Compton effect. The radio lobes, as we discussed in § 2.4, seem to be aligned with the emission that defines the major axis in the X-ray emission, but there are no radio lobes on either the FIRST (White et al. 1998) image or the NVSS (Condon et al. 2002) image that coincide with the X-ray emission features denoted A and B in § 2.4. Therefore, this alignment is probably accidental. Regardless of whether or not we assume the alignment is accidental, the contribution of inverse Compton flux from the radio lobes to the 1–10 keV X-ray emission appears negligible, as there is no (detectable) X-ray enhancement associated with the radio lobes.

Based on the ratio of the D galaxy to NGC 1550 (at the center of an X-ray–bright group; Sun et al. 2003) 20 cm fluxes (56.4 $\pm$ 1.7 mJy/16.6 $\pm$ 1.6 mJy, from the VLA NVSS; Condon et al. 2002) and the measured redshifts, we find that the radio luminosity of the D galaxy in Cl 1205+44 is about 1.4×10^4 times that of NGC 1550. The total radio flux ($\sim 2.5 \times 10^{-14}$ ergs cm^{-2} s^{-1}, assuming a flux spectral index of -0.7 and that the flux extends from 0.1 to 10 GHz) is comparable to the total X-ray flux (and luminosity) of the gas. But if we assume the radio source is only "radio active" (e.g., Lara et al. 2004 and references therein) for 10^8 yr, plus that it probably can inject no more than 10% of its maximum amount of energy output into the ICM, then this reduces the total energy input to 1% of the total energy output of the ICM over 1 Gyr.

Furthermore, there is the lack of a correlation between the radio and the X-ray emission. Therefore, we have no evidence that the radio source is responsible for extra energy input to the ICM of Cl 1205+44. Regardless, Sun et al. (2003) suggest that cD galaxies can provide heating to the ICM via galactic winds over 10 Gyr.

3.5. *Gas Mass and Total Mass*

In order to compare with previous work, it is interesting to calculate the gas mass in various ways. Below we give the

values based on the assumption of a core radius of $21''$. The values are approximately 40% lower if the other best lower limit of $15''$ is used. Therefore, these results are simply for qualitative comparison with previous work.

We used the relationships between X-ray surface brightness and mass as described in Sarazin (1986). We assumed that the electron density is 1.1 times the proton density and a mean molecular weight of 0.6 for the gas. Within 100 kpc for the XMM model, we find a gas mass $\sim 8 \times 10^{11}$ $M_\odot$. Within $1r_c$ the gas mass is 1.9×10^{12}. If we assume no temperature gradient, then we derive a dynamical mass (e.g., Sarazin 1986) of 1×10^{13} $M_\odot$. If we use the Sun et al. (2003) value of M/L of 5 and our value of L_R, then we find that the total galaxy mass of Cl 1205+44 is 7.5×10^{12} $M_\odot$, which is over 10 times higher than their value of about 5×10^{11} $M_\odot$ for the group (*not* classified as a fossil group, however) surrounding NGC 1550. Within 100 kpc, their value of gas mass (M_{gas}) of about 3×10^{11} $M_\odot$ is about 2 times lower than our value for Cl 1205+44. We also calculated M_{2500} from Allen et al. (2001; see also Sun et al. 2003), who derived a formula for M_{2500} using a set of X-ray–luminous relaxed clusters. Then, $M_{2500} = 2.7 \times 10^{13}$ $M_\odot (T/1.37)^{1.5}/E(z) = 3 \times 10^{13}$ $M_\odot$. The expression $E(z) = H/H_0 = [\Omega_{r,0}(1+z)^4 + \Omega_{m,0}(1+z)^3 + \Omega_{\Lambda,0} + (1-\Omega_0)(1+z)^2]^{1/2}$; for $\Omega_{r,0} = 0$, as assumed here, this can be simplified to $(1+z)[1 + z\Omega_{m,0} + \Omega_{\Lambda,0}(1+z)^2 - \Omega_{\Lambda,0}]^{1/2}$.

3.6. *Galaxy Colors*

To compare with other galaxies at this redshift, we have used the Sloan Digital Sky Survey (SDSS)[11] and the 2MASS catalog. For galaxies bright enough to have spectra measured with the SDSS, we find that the colors of those galaxies at z between 0.5 and 0.6 are typical of those in Table 1, which we have assumed to be members of CL 1205+44.

The six galaxies for which we have colors that we associate with Cl 1205+44 are all relatively red, even the late-type galaxies. In contrast, Butcher & Oemler (1984) found a high fraction of *blue* galaxies at this redshift compared to lower redshifts. The Butcher-Oemler effect can be explained by assuming that at 0.6 compared to 0, there is a higher fraction of galaxies that have just fallen into the cluster and have not had their gas stripped yet (e.g., Kauffmann 1995). Hence, the newer (at least spiral) cluster members tend to be bluer, the higher the redshift. For Cl 1205+44, the fossil group could have formed at z of about 2, could have aged about 4 Gyr, and could have had no galaxy infall since birth. The only galaxy population evolution that has taken place has been the merging of galaxies into the central D galaxy plus ram pressure stripping of the gas from the galaxies. Then, there are no recent infall spirals and the spirals have the same colors as the ellipticals (under the assumption that all but galaxy 6 and the AGN in Table 1 are cluster members; for, as noted in § 3.1, it would be peculiar to have the brightest cluster galaxy so far removed from the cluster center). In this hypothesis, the spirals have had their gas removed via ram pressure stripping, and they have been cluster members since its formation approximately 4 Gyr ago. The key issue is what suppresses galaxy infall for fossil groups compared to typical groups and clusters.

Fossil groups have probably formed in initially above-average, overdense regions (so that the group collapsed early), which, however, were not sufficiently rich in matter and galaxies to sustain growth of the group beyond some point in time. The property of having a relatively low total matter value and a
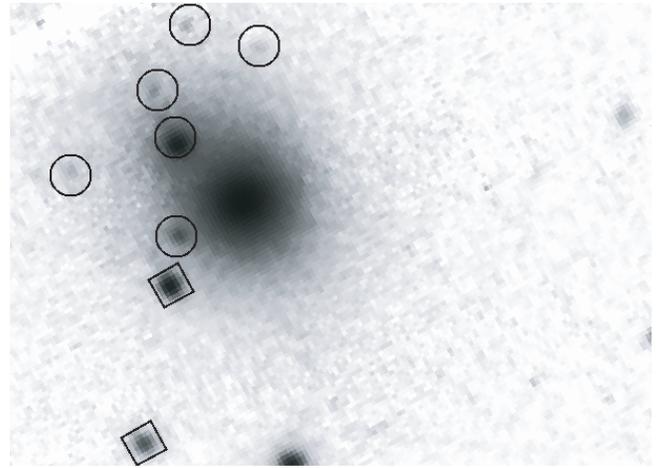

Fig. 13.—*HST* image of the D galaxy area. The objects marked by a square are the galaxies detected in the i'-band data (besides the cD), and the circled objects are resolved in this *HST* image but not in the i'-band image (not shown). North is up, and east is to the left.

negligible blue galaxy fraction is directly related to arriving at an overdensity sufficient for collapse earlier than more massive systems. For example, simulations by Gao et al. (2004) have shown that the galaxy infall rate and number of galaxies in a cluster is related to the age of the universe when the cluster formed; clusters that formed earlier in these simulations tend to have fewer galaxies and less continuous infall (to produce the BO effect) than the systems that formed later. These simulations predict, then, that the galaxy to total cluster mass ratio should be lower for the earliest formed clusters compared to later ones. With a sample of one fossil group with red galaxies, however, it is premature to make a comparison between the data and the simulations at this next level.

3.7. *The D Galaxy*

The D galaxy of our system is similar to the $z = 0.25$–0.5 simulated galaxies in West (1994). Our value of the i' magnitude of 19.27 converts into a rest-frame absolute R_J magnitude of -24.1 (luminosity distance = 3.4×10^3 Mpc, where we used 0.7 for the K-correction for an elliptical at $z = 0.59$). This value -24.1 is about 0.5 mag brighter than the brightest cluster galaxy magnitudes compiled by Collins et al. (2003). Recent galaxy mergers may be responsible for this relatively high brightness.

Moreover, ongoing minor mergers still appear to be visible on the *HST* image (see Fig. 13). These ongoing mergers at a relatively early stage of this fossil group history do not favor the fossil group formation scenario of Mulchaey & Zabludoff (1999), who proposed a formation of these systems with an unusual initial luminosity function. An alternative proposal is the evolutionary scenario of fossil groups proposed by Borne et al. (2000) and Jones et al. (2003). This links compact groups of galaxies and giant elliptical galaxies via an ultraluminous infrared galaxy (ULIRG) phase. The D galaxy of our system (which is also a radio source) has an $i' - K_s$ color very similar to that of ULIRGs (from NED)[12] in the 2MASS survey. This D galaxy could be an ULIRG that is just turning on, except that the K_s-band flux falls well below other ULIRGs (e.g., Yun et al. 2004). Therefore, if the D galaxy were formed in the process suggested by West (1994), then the ULIRG phase has probably already passed.

---

[11] See http://www.sdss.org/dr2.

[12] See http://nedwww.ipac.caltech.edu.

Continuing with the idea of D galaxy evolution in galaxy groups, we refer to Collins et al. (2003). They show that in poor groups the variance between central galaxy properties from group to group is quite large (factors of 10 or more) in terms of total optical output. Thus, we expect that there would be a variation in the optical properties of the D galaxies in fossil groups such as Cl 1205+44, *unless* there is a direct correlation between the kT value and the D galaxy stellar content. However, only a high-redshift ($\gtrsim 0.6$) survey of fossil groups will be able to shed light on the variance of initial conditions, and a survey in general is needed to shed light on the relationship between kT and the D galaxy.

3.8. *Scenarios*

To summarize a formation scenario for Cl 1205+44: there was an initial potential well of dark matter. Energy injection occurred via some process or processes, such as perhaps supernovae, radio galaxies, or ULIRGs. This process heated the gas as galaxies fell into the potential well at a redshift of about 2. The galaxies passed through the ICM several times, and the gas and dust were swept out of the spirals. This ram pressure stripping suppressed continuous star formation and left the spirals to become as red as the ellipticals. The system formed in a relative void of galaxies so that there was no continuous infall of galaxies to keep the system fed with blue spiral field galaxies. The central galaxy grew to become a relatively large D galaxy by merging with other galaxies to form an m_{12} value $\gtrsim 2$. The entire evolutionary sequence took about 4 Gyr.

The above fits with the Jones et al. (2000, 2003) scenario, which is that the time it takes for the merging of galaxies to form a bright central galaxy is approximately 4 Gyr, and no continuous field galaxy infall has taken place. That the D galaxy in Cl 1205+44 appears to have nearly completed the merging process and is approximately 4 Gyr younger than $z \simeq 0$ fossil groups implies that (at least some) fossil groups at $z = 0$ are much older than 4 Gyr.

3.8.1. *Consequences*

Energy to heat the ICM above and beyond gravitational infall results in an entropy (defined here as the pseudoentropy $kT n_e^{-2/3}$, where n_e is the number of electrons cm^{-3} and kT is in keV) floor. The initial energy injection and its consequences were discussed in detail by Babul et al. (2002), who made predictions of initial energy input, which they compared with the data. The two fossil groups found by Jones et al. (2003) with strong enough signal to measure a temperature were consistent with an entropy floor of 100 keV cm^2. In contrast, Cl 1205+44 lies a factor of 2 or more above the 100 keV cm^2 line and instead is nearly on the line occupied by normal rich clusters and normal groups (initial energy input 427 keV cm^2; see Fig. 7). This implies that either Cl 1205+44 is really not a fossil group, contrary to our classification, or that it is unlike the nearby fossil groups, and that we were able to detect Cl 1205+44 precisely because it is much more luminous than the low-z fossil groups. This could be due to the result of a relatively high (compared to the average fossil group) entropy floor input to the ICM, or indicate that Cl 1205+44 simply is more massive that other fossil groups.

In contrast to the model of Babul et al. (2002), we find a much lower value for the pseudoentropy $= T n_e^{-2/3}$ keV cm^2 of 85 keV cm^2. We derived this value at $r = 0.1 r_{200} = 0.1 r_{\rm vir}$ from our β fit ($r_c = 21''$), where we estimate an electron density (and average $kT = 3$ keV) at the core to be $\sim 8.1 \times 10^{-3}$ cm^{-3}, i.e., 6.5×10^{-3} cm^{-3} at $0.1 r_{\rm vir}$. This implies some refinement to the Babul et al. model such as continuous rather than impulsive heating (preheating) at formation. In addition, our entropy for a 3 keV (the temperature of the ICM of Cl 1205+44) temperature is lower than was found for 3 keV virialized objects (including clusters and groups) at $z \lesssim 0.2$ by Ponman et al. (2003).

That the entropy we find is lower than for more nearby clusters and groups at the same temperature is consistent with the "negative" entropy evolution of the suggested by Maughan et al. (2004). Maughan et al. proposed a form $E(z)^{-4/3}$ based on self-similar scaling and the evolution of the critical density of the universe with z. The *scaled-by-temperature* (i.e., divided by kT) entropy for similar temperature objects found by Ponman et al. (2003) at the same radius ($0.1 r_{\rm vir}$) have values of about 75 cm^2, which if scaled from $z = 0$ to 0.5915 by $E(z)^{-4/3} = 49$ cm^2, within a factor of 2 of the value for Cl 1205+44 = 28 cm^2 at $0.1 r_{\rm vir}$. These results then appear to be more consistent with continuous rather than impulsive initial heating to the ICM.

If there were some initial energy injection at $z = 2$ (whatever its cause), then this injection could affect the high-order portion of the CMB via the SZ effect from clusters and groups of galaxies. The possibility of this energy input and its effect on SZ measurements has been discussed by Lin et al. (2004) in the context of deriving cosmological parameters based on the power spectrum of the CMB. Their impulsive heating model requires energy injection at $z = 2$. They fitted their models to the $L_{\rm X}$-$T_{\rm X}$ normal cluster and group data that are shown here in Figure 7, and from this we see that the Cl 1205+44 is consistent with the Lin et al. model (see also Borgani et al. 2004). In addition, that preheating occurred in the Lin et al. model near $z \sim 2$ is consistent with our suggestion that at least some fossil groups, such as Cl 1205+44, formed at $z \sim 2$. However, if continuous heating models can also be shown to fit the data, then the amount of initial impulsive heating suggested by Lin et al. will not be as large as they suggested, and the impact on the high-order CMB observations will be less.

4. SUMMARY AND CONCLUSIONS

To summarize, we have found, via a *ROSAT* survey of archival data, a group of galaxies with a relatively red population. HYPERZ calculations based on the i'- and K_s-band data suggested that the system might have $z \gtrsim 1$. Subsequent redshift work found that the redshift is 0.5915, and *Chandra* plus *XMM-Newton* observations confirmed the existence of an X-ray–emitting gas in the group. We classify this group as a fossil group based on its m_{12} in i' and because its X-ray luminosity exceeds $1 \times 10^{42} \ h_{50}^{-2}$ ergs s^{-1}. This makes it by far the highest redshift fossil group yet reported. The temperature for the ICM is abnormally high compared to two $z \sim 0$ fossil groups with a similar $L_{\rm X\,bol}$, and the $L_{\rm X\,bol}$-L_R point lies approximately halfway between the best-fit lines for normal and fossil groups (Jones et al. 2003). Cl 1205+44 has a kT-$L_{\rm X\,bol}$ value comparable to another $z \sim 0.6$ system that was simply classified as a cluster (RX J0848+4456; Holden et al. 2001). However, although there are some similarities with normal groups and clusters, we have classified it as a fossil group based on the primary criteria of $m_{12} \gtrsim 2$ in R- or V-band rest frame and an X-ray luminosity $\geq 1 \times 10^{42} \ h_{50}^{-2}$.

We conclude that Cl 1205+44 is a fossil group. A formation scenario is that the group formed in peak density region of relatively low total mass at $z \sim 2$. The formation regions did not have enough matter to sustain continuous infall of galaxies and gas, and such a scenario is consistent with the simulation carried out by Gao et al. (2004). Beyond the formation of a central

dominant galaxy via accretion, fossil groups appear old, i.e., fossil-like precisely because they have had little or no evolution in terms of galaxy infall since their inception. In addition, some fossil groups could be considerably older than 4 Gyr. No evolution of the galaxy population (at least in the case of Cl 1205+44) is implied because of the dearth of blue spirals, the kT-$L_{X\,bol}$ value point on the no-evolution tracks for rich clusters of galaxies (Novicki et al. 2002), and our cooling calculations of the IGM are consistent with (but cannot exclude) no significant cooling of CL 1205+44 in 3 Gyr.

Some preheating of the gas in groups and clusters via supernovae or an active galaxy phase is likely to have occurred even in fossil groups (or normal groups), as evidenced by the relatively high temperature of Cl 1205+44, but is also appears that there is continuous rather than impulsive heating at group formation, which results in negative evolution of the pseudo-entropy (e.g., Maughan et al. 2004). However, as the kT versus $L_{X\,bol}$ of Cl 1205+44 fits within 1 σ the no-evolution with z of Novicki et al. (2002), the negative evolution for entropy and the no-evolution models for kT versus $L_{X\,bol}$ (and galaxy population) may need to be fine-tuned to be made consistent with each other.

In addition, the amount of preheating has implications for the interpretation of high-order measurements of the CMB. Our data are consistent with negative evolution of the pseudo-entropy, which implies, on one hand, a lesser impact of the SZ effect from high-z clusters than suggested by Lin et al. (2004). On the other hand, that the kT versus $L_{X\,bol}$ value for our data and many other clusters is consistent with no evolution suggests that perhaps a significant faction of ICM heating did take place

near $z = 2$ and hence does have a significant effect to the high-order terms of the CMB.

The discovery and X-ray and optical measurements of still more $z \geq 0.6$ clusters and fossil groups are needed to develop enough statistics to address the issues of evolution, preheating, and the relationship of fossil group (and cluster) formation to their total mass and galaxy colors.

REFERENCES

Adami, C., Ulmer, M. P., Romer, A. K., Nichol, R. C., Holden, B. P., & Pildis, R. A. 2000, ApJS, 131, 391
Allen, S. W., Schmidt, R. W., & Fabian, A. C. 2001, MNRAS, 328, L37
Babul, A., Balogh, M. L., Lewis, G. F., & Poole, G. B. 2002, MNRAS, 330, 329
Balucinska-Church, M., & McCammon, D. 1992, ApJ, 400, 699
Bertin, E., & Arnouts, S. 1996, A&AS, 117, 393
Borgani, S., et al. 2004, MNRAS, 348, 1078
Borne, K. D., Bushouse, H., Lucas, R. A., & Colina, L. 2000, ApJ, 529, L77
Butcher, H., & Oemler, A. 1984, ApJ, 285, 426
Carilli, C. L., Perley, R. A., & Harris, D. E. 1994, MNRAS, 270, 173
Clarke, T. E., Blanton, E. L., & Sarazin, C. L. 2004, ApJ, 616, 178
Collins, C., Brough, S., Burke, D., Mann, R., & Lynam, P. 2003, Ap&SS, 285, 51
Condon, J. J., Cotton, W. D., Greisen, E. W., Yin, Q. F., Perley, R. A., Taylor, G. B., & Broderick, J. J. 2002, VizieR On-line Data Catalog, 8065, 0
Dickey, J. M., & Lockman, F. J. 1990, ARA&A, 28, 215
Fruchter, A. S., & Hook, R. N. 2002, PASP, 114, 144
Fukazawa, Y., Makishima, K., Tamura, T., Nakazawa, K., Ezawa, H., Ikebe, Y., Kikuchi, K., & Ohashi, T. 2000, MNRAS, 313, 21
Gao, L., White, S. D. M., Jenkins, A., Stoehr, F., & Springel, V. 2004, MNRAS, 355, 819
Harris, D. E., et al. 2000, ApJ, 530, L81
Holden, B. P., et al. 2001, AJ, 122, 629
Jones, L. R., Ponman, T. J., & Forbes, D. A. 2000, MNRAS, 312, 139
Jones, L. R., Ponman, T. J., Horton, A., Babul, A., Ebeling, H., & Burke, D. J. 2003, MNRAS, 343, 627
Kaastra, J. S., & Mewe, R. 1993, A&AS, 97, 443
Kaastra, J. S., et al. 2004, A&A, 413, 415
Kauffmann, G. 1995, MNRAS, 274, 153

Lara, L., Giovannini, G., Cotton, W. D., Feretti, L., Marcaide, J. M., Márquez, I., & Venturi, T. 2004, A&A, 421, 899
Liedahl, D. A., Osterheld, A. L., & Goldstein, W. H. 1995, ApJ, 438, L115
Lin, K., Woo, T., Tseng, Y., Lin, L., & Chiueh, T. 2004, ApJ, 608, L1
Lumb, D. H., Warwick, R. S., Page, M., & De Luca, A. 2002, A&A, 389, 93
Lumb, D. H., et al. 2004, A&A, 420, 853
Maughan, B. J., Jones, L. R., Ebeling, H., & Scharf, C. 2004, MNRAS, 351, 1193
McNamara, B. R., et al. 2000, ApJ, 534, L135
Mulchaey, J. S., Davis, D. S., Mushotzky, R. F., & Burstein, D. 2003, ApJS, 145, 39
Mulchaey, J. S., & Zabludoff, A. I. 1999, ApJ, 514, 133
Nikogossyan, E., Durret, F., Gerbal, D., & Magnard, F. 1999, A&A, 349, 97
Novicki, M. C., Sornig, M., & Henry, J. P. 2002, AJ, 124, 2413
Peterson, J. R., Kahn, S. M., Paerels, F. B. S., Kaastra, J. S., Tamura, T., Bleeker, J. A. M., Ferrigno, C., & Jernigan, J. G. 2004, in The Riddle of Cooling Flows in Galaxies and Clusters of Galaxies, ed. T. Reiprich, J. Kempner, & N. Soker (Charlottesville: Univ. Virginia), 33, http://www.astro.virginia.edu/coolflow/proc.php
Ponman, T. J., Sanderson, A. J. R., & Finoguenov, A. 2003, MNRAS, 343, 331
Romer, A. K., et al. 2000, ApJS, 126, 209
Sarazin, C. L. 1986, Rev. Mod. Phys., 58, 1
Sun, M., Forman, W., Vikhlinin, A., Hornstrup, A., Jones, C., & Murray, S. S. 2003, ApJ, 598, 250
West, M. J. 1994, MNRAS, 268, 79
White, R. L., Becker, R. H., Helfand, D. J., & Gregg, M. D. 1998, VizieR Online Data Catalog, 8051, 0
Yun, M. S., Reddy, N. A., Scoville, N. Z., Frayer, D. T., Robson, E. I., & Tilanus, R. P. J. 2004, ApJ, 601, 723